Identifying and correcting repeat-calling errors in nanopore sequencing of telomeres

Kar-Tong Tan[1,2,3], Michael K. Slevin[1,4], Matthew Meyerson[1,2,3,4,#], Heng Li[5,6,#]
[1]Department of Medical Oncology, Dana-Farber Cancer Institute, Boston, MA, USA
[2]Cancer Program, Broad Institute of MIT and Harvard, Cambridge, MA, USA
[3]Department of Genetics, Harvard Medical School, Boston, MA, USA
[4]Center for Cancer Genomics, Dana-Farber Cancer Institute, Boston, MA, USA
[5]Department of Data Sciences, Dana-Farber Cancer Institute, Boston, MA, USA
[6]Department of Biomedical Informatics, Harvard Medical School, Boston, MA, USA

[#]Correspondence to matthew_meyerson@dfci.harvard.edu or hli@jimmy.harvard.edu

Abstract

Nanopore long-read genome sequencing is emerging as a potential approach for the study of genomes including long repetitive elements like telomeres. Here, we report extensive basecalling induced errors at telomere repeats across nanopore datasets, sequencing platforms, basecallers, and basecalling models. We found that telomeres which are represented by $(TTAGGG)_n$ and $(CCCTAA)_n$ repeats in many organisms were frequently miscalled (~40-50% of reads) as $(TTAAAA)_n$, or as $(CTTCTT)_n$ and $(CCCTGG)_n$ repeats respectively in a strand-specific manner during nanopore sequencing. We showed that this miscalling is likely caused by the high similarity of current profiles between telomeric repeats and these repeat artefacts, leading to mis-assignment of electrical current profiles during basecalling. We further demonstrated that tuning of nanopore basecalling models, and selective application of the tuned models to telomeric reads led to improved recovery and analysis of telomeric regions, with little detected negative impact on basecalling of other genomic regions. Our study thus highlights the importance of verifying nanopore basecalls in long, repetitive, and poorly defined regions of the genome, and showcases how such artefacts in regions like telomeres can potentially be resolved by improvements in nanopore basecalling models.

Keywords

Nanopore-sequencing, long-reads, telomere, basecalling

Background

Telomeres are protective caps found on chromosomal ends, and are known to play critical roles in a wide range of biological processes and human diseases [1,2]. These highly repetitive structures enable cells to deal with the "end-replication problem" through the action of telomerase which adds telomeric repeats to the ends of chromosomes. In cancer, the reactivation of telomerase to drive telomere elongation is estimated to occur in as many as 90% of human cancers, and has been shown experimentally to be critical for malignant transformation [3–8]. As one ages, telomeres are also known to progressively shorten, and are thus thought to also play a central role in the process of aging [9–11]. In many organisms, telomeres are characterized by $(TTAGGG)_n$ repeats that vary in length of between 2 and 20kb long, which are not readily resolved by short-read sequencing approaches. Given the importance of telomeres in a wide range of biological process and the technical challenges associated with their analysis using short-read sequencing, there is significant interest in applying emerging techniques like long-read sequencing to study these repetitive structures.

Long-read sequencing has emerged as a powerful technology for the study of long repetitive elements in the genome. Two main platforms, Single Molecule Real Time (SMRT) sequencing, and Nanopore sequencing, have been developed to generate sequence reads of over 10 kilobases from DNA molecules [12,13]. In SMRT Sequencing, the incorporation of DNA nucleotides is captured real time via one of four different fluorescent dyes attached to each of the four DNA bases, thereby allowing the corresponding DNA sequence to be inferred. Sequencing of the same DNA molecule multiple times in a circular manner further allows highly accurate consensus sequence of the DNA molecule to be generated in a process termed Pacific Biosciences (PacBio) High-Fidelity (HiFi) sequencing [12]. During Nanopore sequencing, the ionic current, which varies according to the DNA sequence, is measured while a single-stranded DNA molecule passes through a nanopore channel. The electrical current measurement is then converted into the corresponding DNA sequence using a deep neural network trained on a collection of ionic current profiles of known DNA sequences [13]. Notably, both platforms enable long DNA molecules of more than 10 kilo-base-pairs to be routinely sequenced and are thus highly suited for the study of long repetitive elements like telomeres.

Results and discussion

In our analysis of telomeric regions with nanopore long-read sequencing in the recently sequenced and assembled CHM13 sample [14,15], we surprisingly observed that telomeric regions were frequently miscalled as other types of repeats in a strand-specific manner. Specifically, although human telomeres are typically represented by $(TTAGGG)_n$ repeats **(Supplementary Figure 1a)**, these regions were frequently recorded as $(TTAAAA)_n$ repeats **(Figure 1a,b, Supplementary Figure 1 and 2a)**. At the same time, when examining the reverse complementary strand of the telomeres which are represented as $(CCCTAA)_n$ repeats, we instead observed frequent substitution of these regions by $(CTTCTT)_n$ and $(CCCTGG)_n$ repeats **(Figure 1a,b, Supplementary Figure 1 and 2b,c)**. Notably, these artefacts were not observed on the CHM13 reference genome [14,15], or PacBio HiFi reads from the same site **(Figure 1a,b)**, suggesting that these observed repeats are artefacts of Nanopore sequencing or the base-calling process, rather than real biological variations of telomeres. Further, these repeat-calling errors could be observed on all chromosomal arms for the CHM13 sample **(Supplementary Figure 1b,c),** and were thus not restricted to a single chromosomal arm. The examination of each telomeric long-read also indicates that these error repeats frequently co-occur with telomeric repeats at the ends of each read **(Figure 1c, Supplementary Figure 3)**.

91 Together, our results suggest that telomeric regions are frequently misrepresented as other
92 types of repeats in a strand-specific manner during Nanopore sequencing.
93
94 We then assessed if these errors are broadly observed in other studies or are specific to the
95 CHM13 dataset from the Telomere-to-Telomere consortium. To assess this, we examined the
96 previously published NA12878 and HG002 Nanopore genome sequencing datasets [12,13,16].
97 Remarkably, the same basecalling errors, TTAGGG→TTAAAA, CCCTAA→CTTCTT, and
98 CCCTAA→CCCTGG, were similarly observed at telomeres in these datasets **(Figure 1d,**
99 **Supplementary Figure 4a)**, suggesting that these basecalling errors at telomeres are broadly
100 observed across multiple studies. Remarkably, between 40-60% of reads at telomeric regions in
101 these three datasets display at least one of these type of basecalling repeat artefacts for the
102 Nanopore sequencing platform **(Supplementary Figure 4b)**, while these errors were not
103 observed in the PacBio HiFi datasets for the same samples **(Supplementary Figure 4b)**.
104 Further, we also partitioned these datasets based on the sequencing platforms used to generate
105 them, and noted that basecalling error repeats are observed across all three nanopore
106 sequencing platforms (MinION, GridION, PromethION) **(Figure 1d, Supplementary Figure 4a)**.
107 Together, these results show that these error repeats extend across nanopore sequencing
108 datasets and sequencing platforms.
109
110 We then questioned if these error repeats are unique to specific nanopore basecallers or
111 basecalling models. We extracted reads from chromosomal ends, and re-basecalled ionic
112 current data of these reads using different basecallers and basecalling models. Using the
113 production-ready basecaller Guppy5 (Oxford Nanopore Technologies), and the developmental-
114 phase basecaller Bonito (Oxford Nanopore Technologies), we noticed that these basecalling
115 error repeats can be readily observed across both basecallers **(Figure 1e, Supplementary**
116 **Figure 5 and 6)**. Further, these error repeats were also observed when different basecalling
117 models were applied **(Figure 1e)**. Significantly, we also observed that the "fast" basecalling
118 mode in Guppy led to almost complete loss of the $(CCCTAA)_n$ strand **(Figure 1e,**
119 **Supplementary Figure 5a)**, while the "HAC" basecalling model enabled both strands to be
120 recovered, highlighting that the basecalling model applied can affect strand-specific recovery of
121 telomeric reads. Together, these results suggest that error repeats are observable across
122 nanopore basecallers, and basecalling models.
123
124 To determine the cause for these repeat-calling errors, we then examined the ionic current
125 profiles of these repeats. We thus generated ionic current profiles of these telomeric repeats
126 and these error repeats, induced by the nanopore basecallers, using known mean current
127 values of different 6-mers **(Methods)**. Remarkably, we observed a high degree of similarity
128 between current profiles between telomeric repeats and these basecalling errors **(Figure 1f)**.
129 Specifically, we observed that $(TTAGGG)_n$ telomeric repeats had a high degree of similarity with
130 the $(TTAAAA)_n$ error repeats generated by the Bonito base-caller (Pearson correlation = 0.9928,
131 Euclidean distance=4.9934) **(Supplementary Figure 7a-c)**. Similarly, $(CCCTAA)_n$ current
132 profile also showed high similarity with $(CCCTGG)_n$ repeats (Pearson correlation = 0.9783,
133 Euclidean distance = 4.687), and reasonably good similarity with $(CTTCTT)_n$ repeats (Pearson
134 correlation = 0.6411, Euclidean distance = 19.384) **(Supplementary Figure 7a-c)**,. Together,
135 these results suggest that similarities in current profiles between repeat sequences are possible
136 causes for repeat-calling errors at telomeric repeats.
137
138 We then examined if repeat-calling errors may extend to other repetitive sequences beyond
139 telomeric sequences. To address this, we search for other repeat pairs with similar current
140 profiles that may be susceptible to these repeat-calling errors. We simulated and performed
141 pairwise comparison of current profiles for all 6-mer repeats (n=8,386,560 comparisons)

142 **(Methods)**. Using similar Pearson correlation (≥0.99) and Euclidean distance cutoffs (≤5) as
143 observed for telomeric repeat errors identified in this study **(Supplementary Figure 7a-c)**, we
144 identified a further 2577 pairs of repeats with similar current profiles **(Supplementary Table 1,**
145 **Supplementary Figure 7d)**. For instance, we found that $(TTAGGG)_n$ telomeric repeats also
146 showed high similarities in current profiles with repeats with single-nucleotide substitutions like
147 $(TTA\underline{A}GG)_n$, $(TTAG\underline{A}G)_n$ and $(TT\underline{G}GGG)_n$ **(Supplementary Figure 7d,e)**. Repeat sequences
148 like $(GCTGCT)_n$ and $(\underline{AAC}G\underline{GC})_n$ that differed drastically at the sequence level, but shared
149 similar current profiles were also observed **(Supplementary Figure 7d,f)**. Further, we also
150 examined the unmappable pool of CHM13 nanopore reads after mapping it to the CHM13
151 reference assembly. Remarkably, a significant pool of reads with long $(GT)_n$ repeats were
152 readily observed **(Supplementary Figure 8)**. Interestingly, $(GTGTGT)_n$ repeats were also found
153 to have high similarities in current profiles with $(CTCTCT)_n$ repeats **(Supplementary Figure 7d,**
154 **Supplementary Table 1)**, suggesting that the pool of unmappable $(GT)_n$ reads may include
155 $(CT)_n$ repeats. Collectively, our results suggests that these basecalling error repeats may be
156 observed at other repetitive regions, beyond telomeres.
157
158 To resolve these basecalling errors at telomeres, we then attempted to tune the nanopore
159 basecaller by providing it with more training examples of telomeres **(Figure 2a)**. Notably, model
160 training was performed with a low learning rate to ensure that the majority of the model does not
161 get affected during training while ensuring that minor adjustments in the model can be made to
162 accurately basecall telomeres. Specifically, we tuned the deep neural network model underlying
163 the Bonito basecaller by training it at a low learning rate with ground truth telomeric sequences
164 extracted from the CHM13 reference genome, and current data of the corresponding reads
165 **(Methods)**. As two Nanopore PromethION runs were performed on the CHM13 dataset, we
166 used the data from one run for training (run225) and tuning of the basecaller, and held out the
167 data from the second run (run 226) for evaluation of our tuned basecaller. With this approach,
168 we see a significant improvement in the base-calls of both the telomeres, and sub-telomeric
169 regions on the training data and held out dataset with clearly observable decrease in errors on
170 the chromosomal ends **(Figure 2b, Supplementary Figure 9a-d)**. Together, our results indicate
171 that a nanopore base-caller can be tuned to more accurately base-call telomeric regions by
172 providing additional training examples.
173
174 As it is computationally more efficient to redo repeat-calling only for the small fraction of
175 problematic telomeric reads rather than all reads, we developed an overall strategy to select
176 these telomeric reads for re-basecalling with the tuned Bonito+telomeres basecaller **(Figure 2c)**.
177 To select telomeric reads for selective re-basecalling, we relied on an observation from the
178 CHM13 reference genome and nanopore sequencing datasets. Specifically, we noticed that
179 telomeric reads which maps to the ends of the CHM13 reference genome tend to show a high
180 frequency of telomeric, or basecalling error repeats as compared to the rest of the genome
181 **(Supplementary Figure 10)**. We therefore utilized this observation to separate the non-
182 telomeric reads, from the candidate telomeric reads **(Figure 2c, Methods)**. These telomeric
183 reads were then re-base-called with the tuned Bonito basecaller before being recombined with
184 the pool of non-telomeric reads. Remarkably, with this strategy, we observed a significant
185 improvement in recovery of telomeric reads with $(TTAGGG)_n$ and $(CCCTAA)_n$ repeats (from 384
186 to 476 TTAGGG and 373 to 686 CCCTAA reads) **(Figure 2d)**. At the same time, a sharp
187 reduction of these basecalling repeat errors was also observed (151 to 17 TTAAAA reads, 561
188 to 48 CTTCTT reads, and 337 to 20 CCCTGG reads) **(Figure 2d)**. Together, these results
189 suggests that our "selective tuning" approach for fixing basecalling errors at telomeres can
190 improve recovery of telomeric reads while reducing telomeric basecalling repeat artefacts.
191

192   We further evaluated our approach for possible impact on overall basecalling accuracy. While a
193   reduction in global basecalling accuracy was observed (~1-2%) when our tuned basecaller was
194   directly applied to the full dataset, caused likely by miscalling of endogenous $(CTTCTT)_n$
195   genomic repeats as $(CCCTAA)_n$, this loss of global basecalling accuracy could be avoided by
196   applying our basecaller to telomeric reads alone. Concordant with this, we did not observe
197   changes in overall basecalling accuracy with our telomere-selective tuning approach **(Figure
198   2e)**. These results indicate that our telomere-selective tuning approach has negligible impact on
199   basecalling accuracy for the rest of the genome.
200
201
202   **Conclusion**
203
204   In this study, we showed that basecalling errors can be widely observed at telomeric regions
205   across nanopore datasets, sequencing platforms, basecallers, and basecalling models. We
206   further showed that these strand-specific basecalling errors were likely induced by similarities in
207   current profiles between different repeat types. To resolve these basecalling errors at telomeres,
208   we devised an overall strategy to re-basecall telomeric reads using a tuned nanopore basecaller.
209   More broadly, our study highlights the importance of verifying nanopore basecalls in long,
210   repetitive and poorly defined regions of the genome. For instance, this can be done either with
211   an orthogonal platform, or at a minimum by ensuring nanopore basecalls between opposite
212   strands are concordant. In the future, we anticipate that further improvements in the nanopore
213   basecaller or basecalling model as demonstrated in this study will potentially lead to the
214   reduction or elimination of these basecalling artefacts.
215
216

Methods

Nanopore and PacBio Datasets
Nanopore and PacBio HiFi datasets for the CHM13 sample were downloaded directly from the telomere-to-telomere consortium (https://github.com/marbl/CHM13)

Nanopore dataset for GM12878 was obtained from the Nanopore WGS consortium (https://github.com/nanopore-wgs-consortium/NA12878/blob/master/Genome.md). PacBio HiFi dataset for GM12878 was obtained from the repository at the SRA database (SRP194450), and downloaded from the following link (https://www.ebi.ac.uk/ena/browser/view/SRR9001768?show=reads)

The HG002 PacBio HiFi and Nanopore datasets were downloaded from the Human Pangenome Reference Consortium (https://github.com/human-pangenomics/HG002_Data_Freeze_v1.0). Specifically, the HG002 Data Freeze (v1.0) recommended downsampled data mix was downloaded. The PacBio HiFi dataset corresponds to ~34X coverage of Sequel II System with Chemistry 2.0. The Nanopore dataset corresponds to 60x coverage of unsheared sequencing from 3 PromethION flow cells from Shafin et al [17].

Extraction of candidate telomeric reads
Telomeric reads were extracted by mapping all reads to the CHM13 draft genome assembly (v1.0) obtained from the telomere-to-telomere consortium using Minimap2 (version 2.17-r941). Subsequent to that, reads that mapped to within 10 kilobasepairs of the start and end of each autosome and X-chromosome were then extracted using SAMtools (version 1.10).

Co-occurrence matrix
Candidate PacBio HiFi and Nanopore telomeric reads were first extracted as described above, and then converted into the FASTA format using SAMtools (version 1.10). Subsequent to that, custom Python scripts were used to assess if each of the reads contain at least four consecutive counts of the repeat sequence of interest (e.g. $(TTAGGG)_4$). This information is then used to generate a pair-wise correlation matrix as depicted with R in the main text.

Basecalling of nanopore data with different basecallers and basecalling models
Basecalling of Nanopore data was done using Guppy (Version 4.4.2), Guppy (Version 5.0.16) and Bonito v0.3.5 (commit d8ae5eeb834d4fa05b441dc8f034ee04cb704c69). For Guppy4, four different basecalling models were applied (guppy_dna_r9.4.1_450bps_fast, guppy_dna_r9.4.1_450bps_hac, guppy_dna_r9.4.1_450bps_prom_fast, guppy_dna_r9.4.1_450bps_prom_hac). For Guppy 5, six different basecalling models were applied (dna_r9.4.1_450bps_fast, dna_r9.4.1_450bps_hac, dna_r9.4.1_450bps_sup, dna_r9.4.1_450bps_fast_prom, dna_r9.4.1_450bps_hac_prom, dna_r9.4.1_450bps_sup_prom) For Bonito, the v1, v2, v3, v3.1 and default basecalling models were applied.

Current profiles for different repeat sequences
The mean current level for different k-mers sequenced by Nanopore sequencing was obtained from the k-mer models published by Oxford Nanopore (https://github.com/nanoporetech/kmer_models/tree/master/r9.4_180mv_450bps_6mer). Circular permutations of each 6-mer of interest was generated, and their corresponding mean current level extracted from the k-mer models. The current profiles for each of the indicated repeat sequences were then plotted and depicted in the figure.

268 ***Pairwise comparison of all possible k-mers***
269 Current profile for each 6-mer repeat sequence was generated using the published k-mer
270 models as described above. Pairwise comparisons of all possible 6-mer repeat current profiles
271 was then performed (8,386,560 pairs in total). A corresponding (i) Pearson correlation value, (ii)
272 mean-centered Euclidean distance, and (iii) mean current difference for each pair of 6-mer
273 repeat current profiles were then generated. Pairs of repeats with a Pearson correlation value ≥
274 0.99 and Euclidean distance ≤ 5 were selected as putative repeat pairs that can be miscalled.
275

276 ***Tuning of bonito model***
277 The default model from Bonito v0.3.5 (commit d8ae5eeb834d4fa05b441dc8f034ee04cb704c69)
278 was used as the base model for model tuning. The training dataset needed for the training
279 process was generated from the telomeric reads from a PromethION run in the CHM13 dataset
280 (run225). More broadly, we then generate the training dataset by matching the current profiles
281 from the Nanopore run to ground truth sequences that we extracted from the CHM13 draft
282 reference genome assembly (v1.0) using custom written code.
283

284 Specifically, these telomeric reads were first basecalled using the initial Bonito basecalling
285 model, and then mapped back to the CHM13 draft reference genome assembly (v1.0). This
286 allowed each telomeric read to be properly assigned to its corresponding chromosomal arm with
287 its sub-telomeric sequence. Nonetheless, as the telomeric region of the same read could not be
288 properly mapped to the telomeric repeats due to the repeat errors, there was difficulty in
289 assigning the nanopore current data to the correct ground truth sequences in the reference
290 genome. As such, the presume length of sequences to extract was estimated using the
291 basecalling repeat error sequences, and the same length of sequences were then extracted
292 from the CHM13 reference genome to serve as ground truth sequences. With this idea and with
293 custom Perl script, we were able to generate a set of ground truth sequences and signals for
294 model tuning. These data were then formatted into the corresponding python objects required
295 by the Bonito basecaller with custom Python scripts. Using the tune function in Bonito and with
296 our prepared training dataset, we were then able to train the basecaller to convergence.
297

298 ***Selective application of tuned basecaller to telomeric reads***
299 We applied our tuned basecaller by first extracting candidate telomeric reads for re-basecalling.
300 This was done by enumerating the total 3-mer telomeric (TTAGGG, CCCTAA) and repeat
301 artefact count (TTAAAA, CTTCTT, CCCTGG) on each read. Reads with at least 10 total counts
302 of these repeats were isolated and their readnames noted. These reads were then excluded
303 from the total pool of reads via their readnames, and basecalled separately using our tuned
304 basecaller using the fast5 data of these reads. Following basecalling with the tuned basecaller,
305 these reads were then recombined with the main pool of reads.
306
307
308
309 **Abbreviations**
310 PacBio: Pacific Biosciences
311 SMRT: Single Molecule Real Time
312
313

Author information

Affiliations

Department of Medical Oncology, Dana-Farber Cancer Institute, Boston, MA, USA
Kar-Tong Tan, Michael K. Slevin, Matthew Meyerson

Cancer Program, Broad Institute of MIT and Harvard, Cambridge, MA, USA
Kar-Tong Tan, Matthew Meyerson

Department of Genetics, Harvard Medical School, Boston, MA, USA
Kar-Tong Tan, Matthew Meyerson

Center for Cancer Genomics, Dana-Farber Cancer Institute, Boston, MA, USA
Michael K. Slevin, Matthew Meyerson

Department of Data Sciences, Dana-Farber Cancer Institute, Boston, MA, USA
Heng Li

Department of Biomedical Informatics, Harvard Medical School, Boston, MA, USA
Heng Li

Author contributions
K.T.T. and M.S. identified issues with Nanopore sequencing of telomeres, and discovered basecalling errors at telomeric regions. K.T.T. evaluated basecalling errors in Nanopore sequencing datasets, and designed the overall approach for correcting basecalling errors at telomeric regions with inputs from H.L. and M.M. K.T.T. wrote the initial draft of the manuscript with inputs from H.L. and M.M. M.M. and H.L. jointly supervised the work. All authors read, revised, and approved the submission of the manuscript.

Corresponding authors
Correspondence to Matthew Meyerson (matthew_meyerson@dfci.harvard.edu) or Heng Li (hli@jimmy.harvard.edu).

Declarations

Ethics approval and consent to participate
Not applicable.

Consent for publication
Not applicable.

Availability of data and materials
Source code to apply and retrain the bonito bascalling model for telomeric region can be found at the following link: https://github.com/ktan8/nanopore_telomere_basecall/.

The tuned bonito basecalling model can be downloaded from https://zenodo.org/api/files/86cb9586-300f-493d-b9c4-0ab2f2848e3c/chm13_nanopore_trained_run225.zip. A comprehensive version of Supplementary Table 1 with all possible pairs of k-mers can be found at https://zenodo.org/api/files/86cb9586-300f-493d-b9c4-0ab2f2848e3c/all_comparisions.similar_profile.txt.zip.

Competing interests
H.L. is a consultant of Integrated DNA Technologies and on the SAB of Sentieon, Innozeen and BGI. M.M. has a patent for *EGFR* mutations for lung cancer diagnosis issued, licensed, and with royalties paid from LabCorp and a patent for EGFR inhibitors pending to Bayer; and was a founding advisor of, consultant to, and equity holder in Foundation Medicine, shares of which were sold to Roche.

References

1. Shay JW, Wright WE. Telomeres and telomerase: three decades of progress. Nat Rev Genet. 2019;

2. Turner K, Vasu V, Griffin D. Telomere Biology and Human Phenotype. Cells. 2019;

3. Li Y, Tergaonkar V. Noncanonical functions of telomerase: Implications in telomerase-targeted cancer therapies. Cancer Res. 2014.

4. Kim NW, Piatyszek MA, Prowse KR, Harley CB, West MD, Ho PLC, et al. Specific association of human telomerase activity with immortal cells and cancer. Science (80-). 1994;

5. Meyerson M, Counter CM, Eaton EN, Ellisen LW, Steiner P, Caddle SD, et al. hEST2, the putative human telomerase catalytic subunit gene, is up- regulated in tumor cells and during immortalization. Cell. 1997;

6. Kolquist KA, Ellisen LW, Counter CM, Meyerson M, Tan LK, Weinberg RA, et al. Expression of TERT in early premalignant lesions and a subset of cells in normal tissues. Nat Genet. 1998;

7. Li Y, Tergaonkar V. Telomerase reactivation in cancers: Mechanisms that govern transcriptional activation of the wild-type vs. mutant TERT promoters. Transcription. 2016.

8. Yuan X, Larsson C, Xu D. Mechanisms underlying the activation of TERT transcription and telomerase activity in human cancer: old actors and new players. Oncogene. 2019.

9. Shay JW. Telomeres and aging. Curr. Opin. Cell Biol. 2018.

10. Aubert G, Lansdorp PM. Telomeres and aging. Physiol. Rev. 2008.

11. Shammas MA. Telomeres, lifestyle, cancer, and aging. Curr Opin Clin Nutr Metab Care. 2011;

12. Wenger AM, Peluso P, Rowell WJ, Chang PC, Hall RJ, Concepcion GT, et al. Accurate circular consensus long-read sequencing improves variant detection and assembly of a human genome. Nat Biotechnol. 2019;

13. Jain M, Koren S, Miga KH, Quick J, Rand AC, Sasani TA, et al. Nanopore sequencing and assembly of a human genome with ultra-long reads. Nat Biotechnol. 2018;

14. Miga KH, Koren S, Rhie A, Vollger MR, Gershman A, Bzikadze A, et al. Telomere-to-telomere assembly of a complete human X chromosome. bioRxiv. 2019;

15. Logsdon GA, Vollger MR, Hsieh PH, Mao Y, Liskovykh MA, Koren S, et al. The structure, function and evolution of a complete human chromosome 8. Nature. 2021;

16. Zook JM, Catoe D, McDaniel J, Vang L, Spies N, Sidow A, et al. Extensive sequencing of seven human genomes to characterize benchmark reference materials. Sci Data. 2016;

17. Shafin K, Pesout T, Lorig-Roach R, Haukness M, Olsen HE, Bosworth C, et al. Nanopore sequencing and the Shasta toolkit enable efficient de novo assembly of eleven human genomes. Nat Biotechnol. 2020;38.
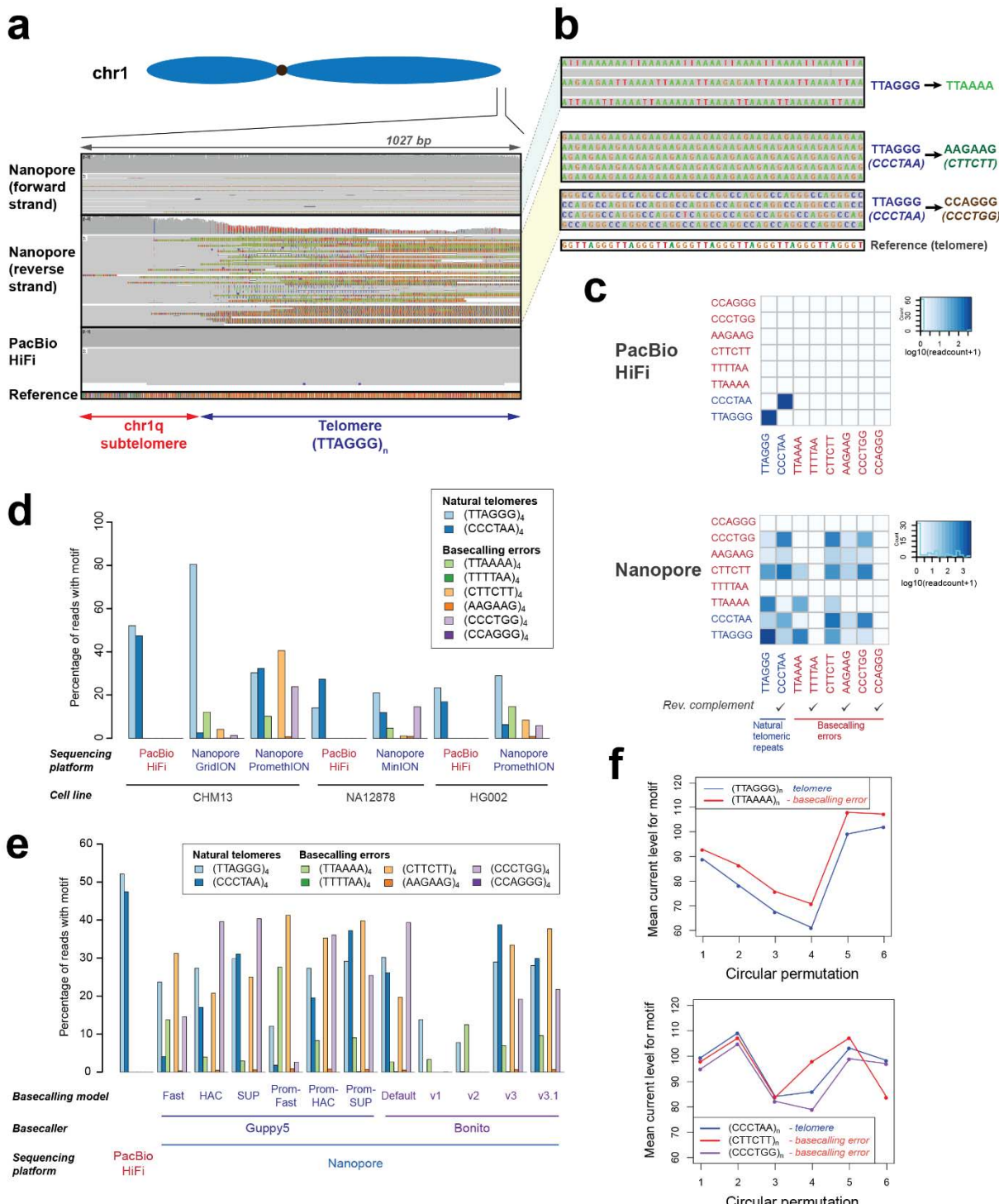
Figure 1

428
Figure 1 Strand-specific Nanopore basecalling errors are pervasive at telomeres. (a,b)
IGV screenshot illustrating the three types of basecalling errors found on the forward and
reverse strands of telomeres for Nanopore sequencing. $(TTAGGG)_n$ on the forward strand of
Nanopore sequencing data was basecalled as $(TTAAAA)_n$ while $(CCCTAA)_n$ on the reverse

433 strand was basecalled as $(CTTCTT)_n$ and $(CCCTGG)_n$. PacBio HiFi data generated from the
434 same cell line (CHM13) is depicted as a control. Reference genome indicated in the plot
435 corresponds to the chm13 draft genome assembly (v1.0). **(c)** Co-occurrence heatmap
436 illustrating the frequency of co-occurrence of repeats corresponding to natural telomeres, or to
437 basecalling errors in PacBio HiFi and Nanopore long-reads found at chromosomal ends (within
438 10kb of annotated end of the reference genome). Diagonal of co-occurrence matrix represents
439 counts of long-reads with only a single type of repeats observed. **(d)** Basecalling errors at
440 telomeres are observed across different nanopore datasets and sequencing platforms. **(e)**
441 Basecalling errors at telomeres are observed different nanopore basecallers and basecalling
442 models. Guppy5 and the Bonito basecallers, and different bascalling models for each bascaller,
443 were used to basecall telomeric reads in the CHM13 PromethION dataset (reads that mapped
444 to flanking 10kb regions of the CHM13 reference genome). **(f)** Basecalling errors share similar
445 nanopore current profiles as telomeric repeats. Current profiles for telomeric and basecalling
446 error repeats were plotted based on known mean current profiles for each k-mer (Methods).
447
448

Figure 2
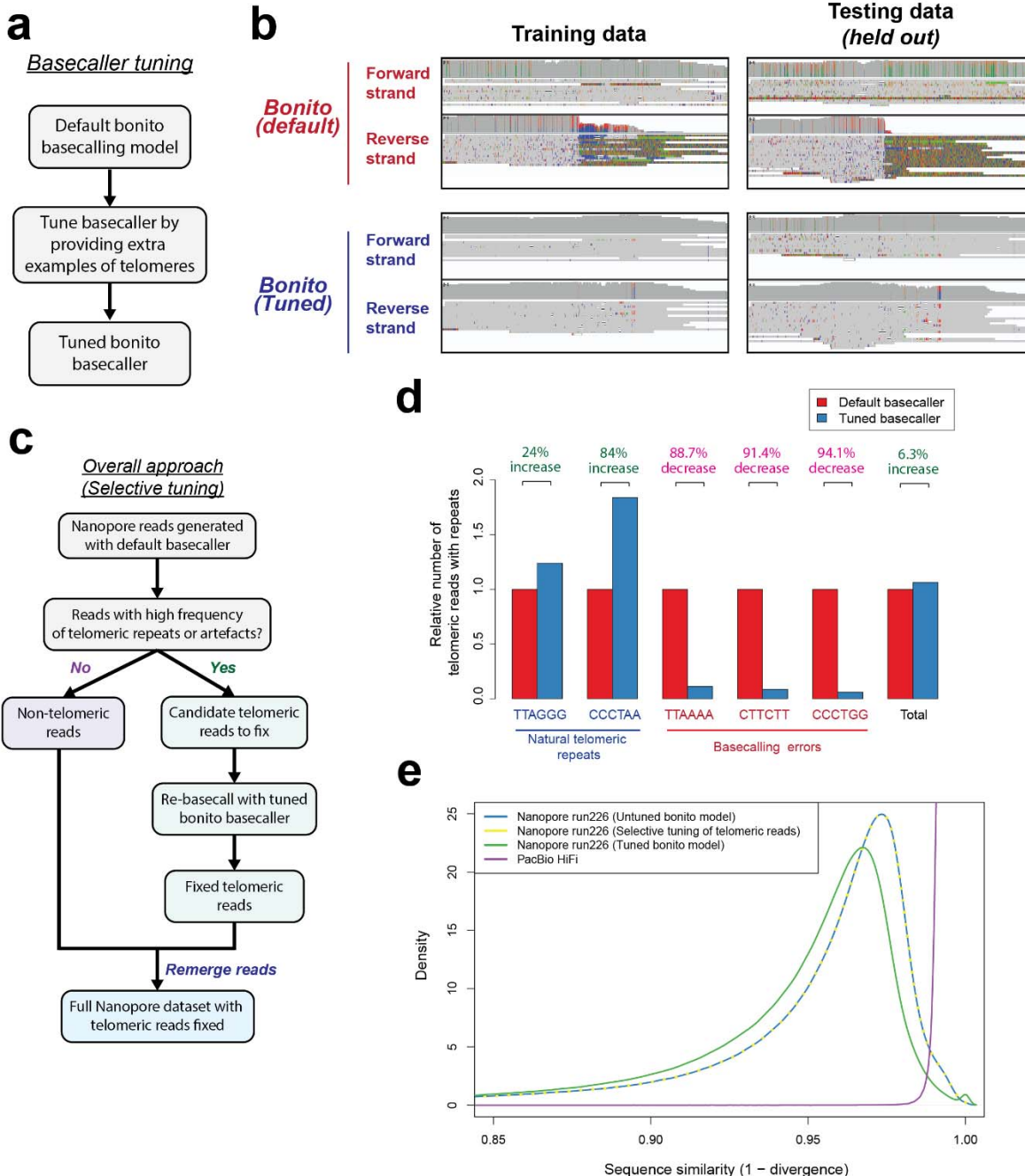
Figure 2 Selective re-basecalling of telomeric reads resolves basecalling errors at telomeres. (a) Approach for tuning the bonito basecalling model for improving basecalls at telomeres. **(b)** Tuned bonito basecalling model leads to improvement in basecalls at telomeric regions. IGV screenshots of telomeric region (chr2q) in the CHM13 dataset basecalled using the default bonito basecaller, and the tuned bonito basecalling model is as depicted. **(c)** Overall approach for selecting and fixing telomeric reads in nanopore sequencing datasets. Telomeric reads are selected (Methods), and rebasecalled using the tuned bonito basecalling model. **(d)** The selective tuning approach leads to improved recovery of telomeric reads, and decrease in

13

458   the number of reads with basecalling artefacts. Evaluation was performed on the held out test
459   dataset (run226). **(e)** The 'selective basecalling' approach leads to little detected negative
460   impact on basecalling of other genomic regions. The sequence similarity of all reads to the
461   reference genome for three approaches for basecalling of nanopore reads was evaluated. They
462   are applying the default bonito basecalling model to all reads (untuned bonito model), applying
463   the tuned bonito basecalling model to all reads (tuned bonito model), and applying the tuned
464   bonito basecalling model selectively to telomeric reads only (selective tuning of telomeric reads).
465   The density plot depicts the sequence similarity of each read against the CHM13 reference
466   genome as assessed using minimap2.
467

Supplementary Figure 1
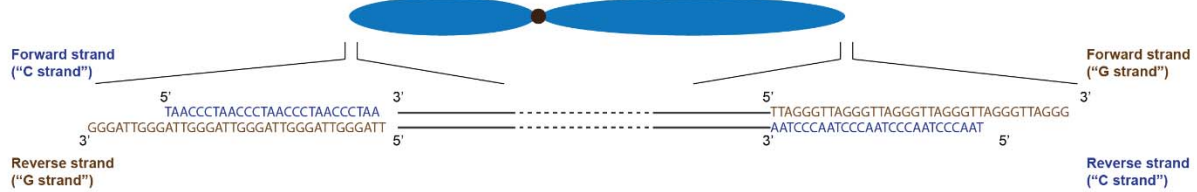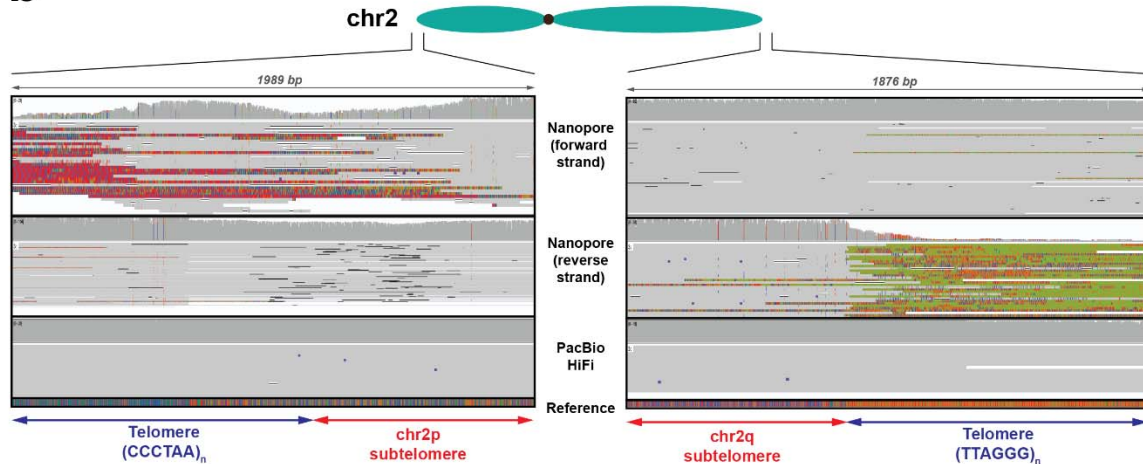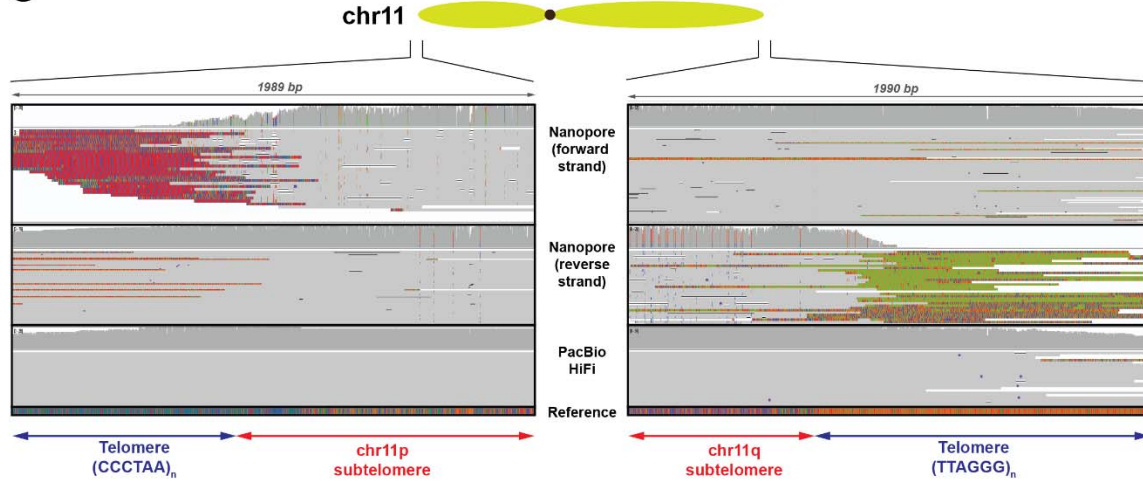
Supplementary Figure 1 Additional screenshots of basecalling repeat errors found on different chromosomal arms. (a) Schematic depicting sequence and orientation of telomeric repeat sequences on the p-arms (arm on the left in the schematic) and q-arms (arm on the right of the schematic) of a chromosome. Note that the forward strand for the arm on the left, and reverse strand for the arm on the right are "C-rich strands" and characterized by $(CCCTAA)_n$ repeats in a 5'-to-3' direction. Also note that the reverse strand for the arm on the left, and forward strand for the arm on the right are "G-rich strands" and characterized $(TTAGGG)_n$

477   repeats in a 5'-to-3' direction. **(b-c) S**creenshots depicting additional representative examples of
478   chromosomal arms with basecalling error repeats.   These are **(b)** chromosome 2 and **(c)**
479   chromosome 11. Screenshots were extracted from the Integrative Genomics Viewer for the
480   CHM13 long-read dataset mapped against the CHM13 reference genome. Related to Figure 1a.
481

Supplementary Figure 2

a

>0e88dfbf-3bd8-4fa9-a35e-d7b510377e6e (+) 9237 bp, chr1q

TTAGGG → TTAAAA

b

>2e9951c6-e9dd-4c87-8470-078b4cbffd84 (-) 42471 bp, chr1q

TTAGGG → AAGAAG
(CCCTAA)   (CTTCTT)

c

>5270195c-c854-4c76-850c-a4ec17090fdd (-) 3515 bp, chr1q

TTAGGG → CCAGGG
(CCCTAA)   (CCCTGG)

Supplementary Figure 2 Examples of long-reads with three types of basecalling error repeats found at telomeres. (a-c) Sequences and readnames of representative long-reads with the three reported types of basecalling error repeats are as depicted. The region with the basecalling error repeats is highlighted in red. The three type of basecalling errors found on each long read are **(a)** $(TTAGGG)_n$ to $(TTAAAA)_n$, **(b)** $(CCCTAA)_n$ to $(CTTCTT)_n$ and **(c)**

17

488   (CCCTAA)$_n$ to (CCCTGG)$_n$. Note that **(b)** and **(c)** represents the reverse complementary
489   sequence of the actual nanopore long-read sequence. Also note that the repeats were found on
490   the end of each read as expected given that telomeric repeats are typically found on the end of
491   the chromosomes.
492
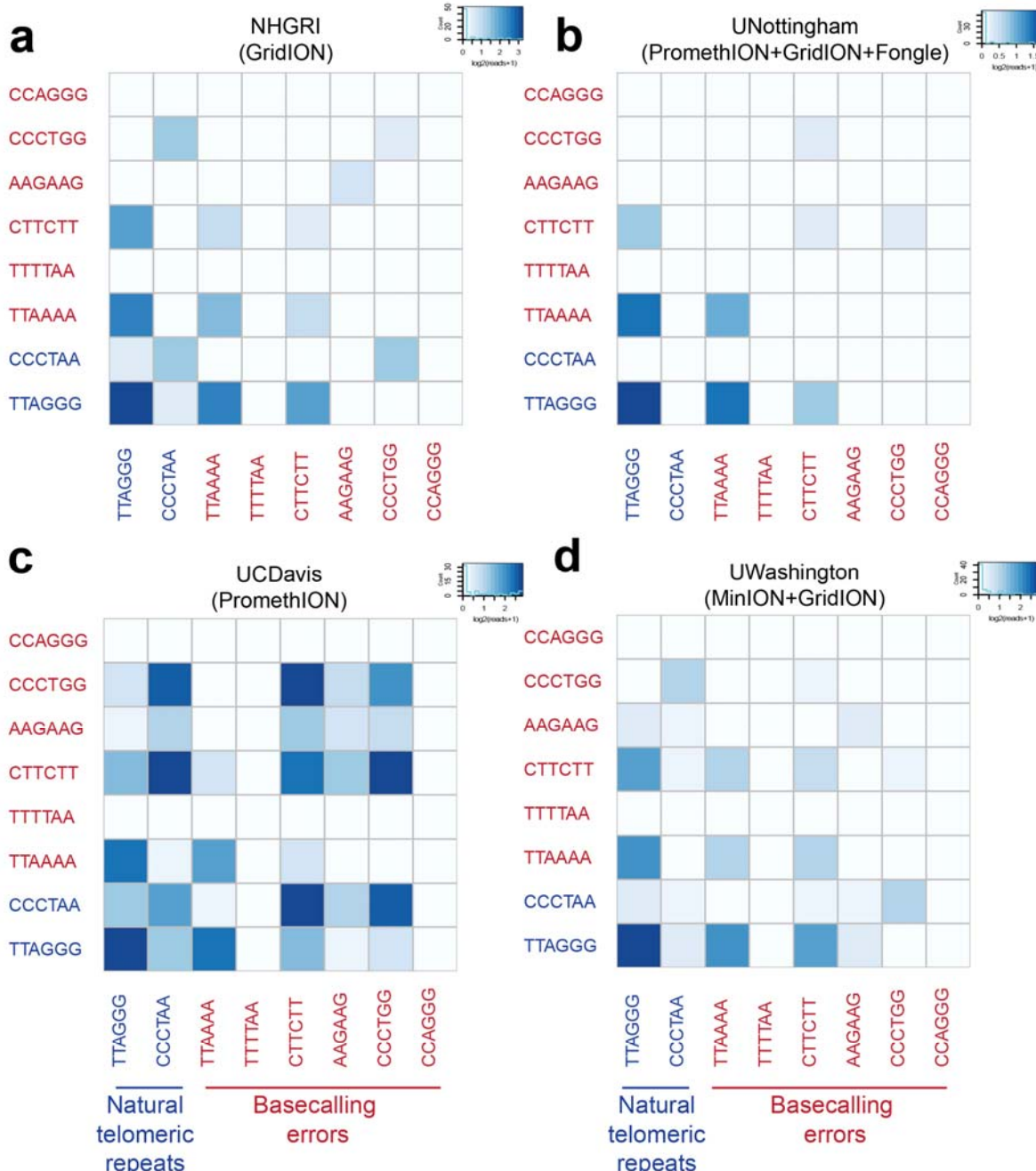
Supplementary Figure 3 Co-occurrence heatmap illustrating the frequency of co-occurrence of telomeric repeats and basecalling errors for the CHM13 Nanopore dataset generated at different sites. These are **(a)** National Human Genome Research Institute (NHGRI), **(b)** University of Nottingham (UNottingham), **(c)** University of California, Davis (UCDavis) and **(d)** University of Washington (UWashington). The sequencing platforms used for sequencing at each of the sites are also as indicated. This figure is related to Figure 1b.

Supplementary Figure 4
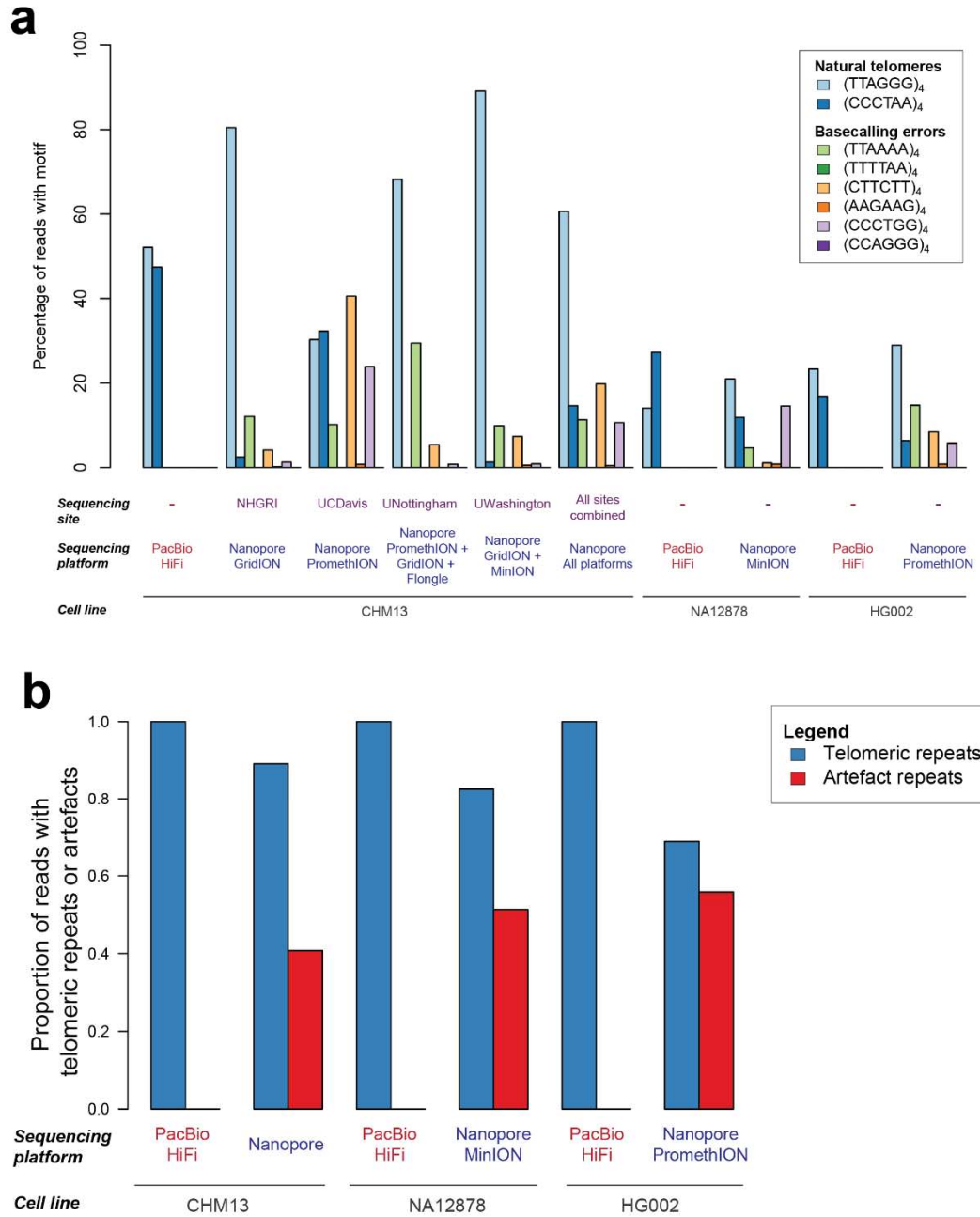
Supplementary Figure 4 Frequency of telomeric repeat errors in different Nanopore sequencing dataset and sequencing platforms. (a) Frequency of basecalling error repeats on three different cell lines generated by different Nanopore sequencing platforms. This figure is an extension Figure 1d. **(b)** Aggregated fraction of basecalling error repeats for different cell lines and datasets.

20

Supplementary Figure 5

a

b
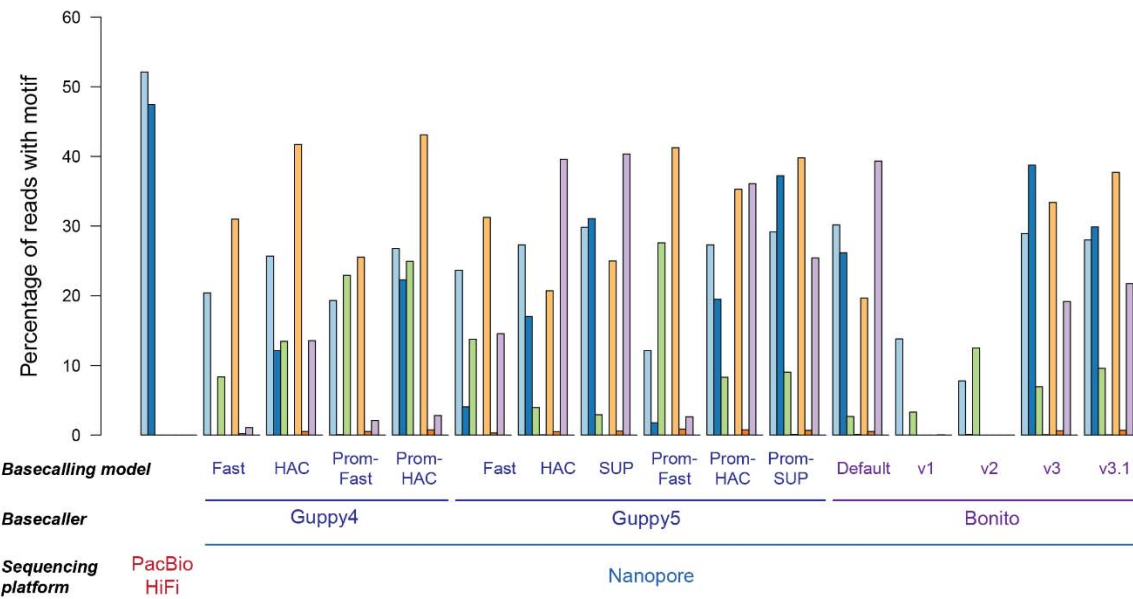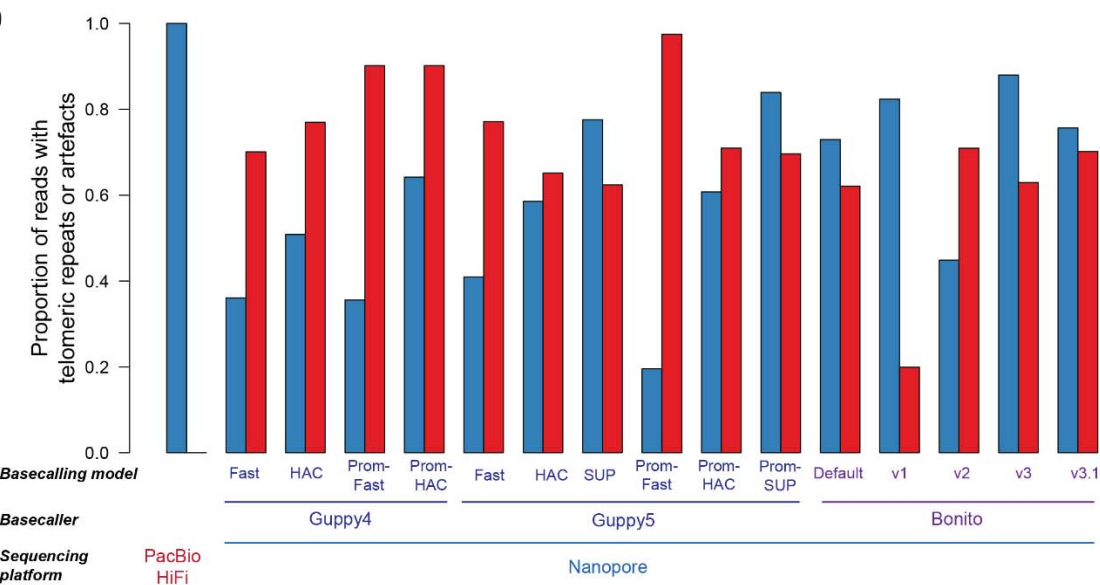
Supplementary Figure 5 Frequency of telomeric repeat errors in different Nanopore basecallers. (a) Frequency of basecalling error repeats for different basecallers (Guppy4, Guppy5 and Bonito) and basecalling models. This figure is an extension of Figure 1e. **(b)** Aggregated fraction of basecalling error repeats for different basecallers and basecalling models.
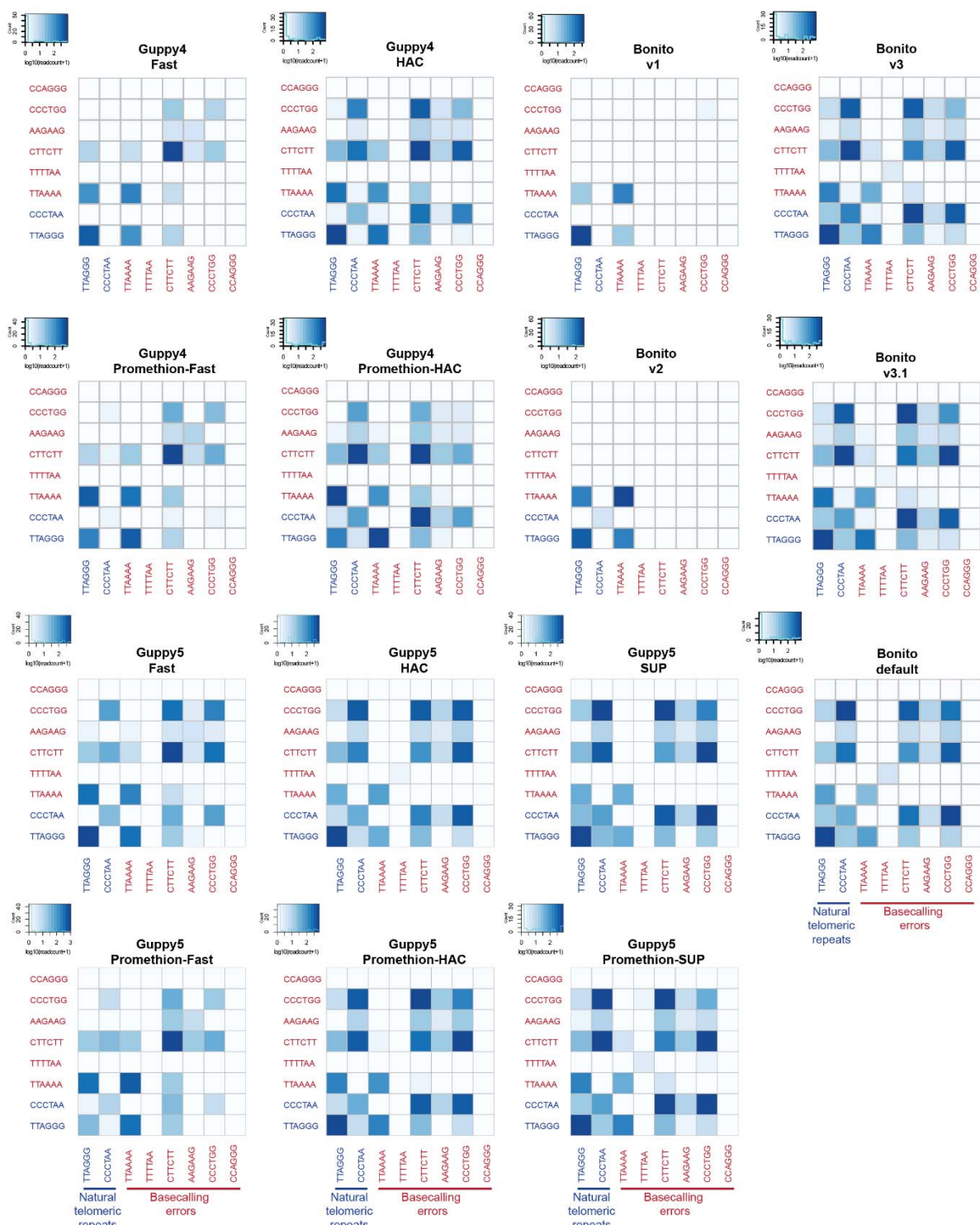
21

Supplementary Figure 6

Supplementary Figure 6 Co-occurrence heatmap for different Nanopore basecalling models. Different nanopore basecallers and basecalling models were applied to the CHM13 Nanopore promethion datasets. The frequency of telomeric repeats and basecalling artefacts observed on reads obtained are as depicted.

22
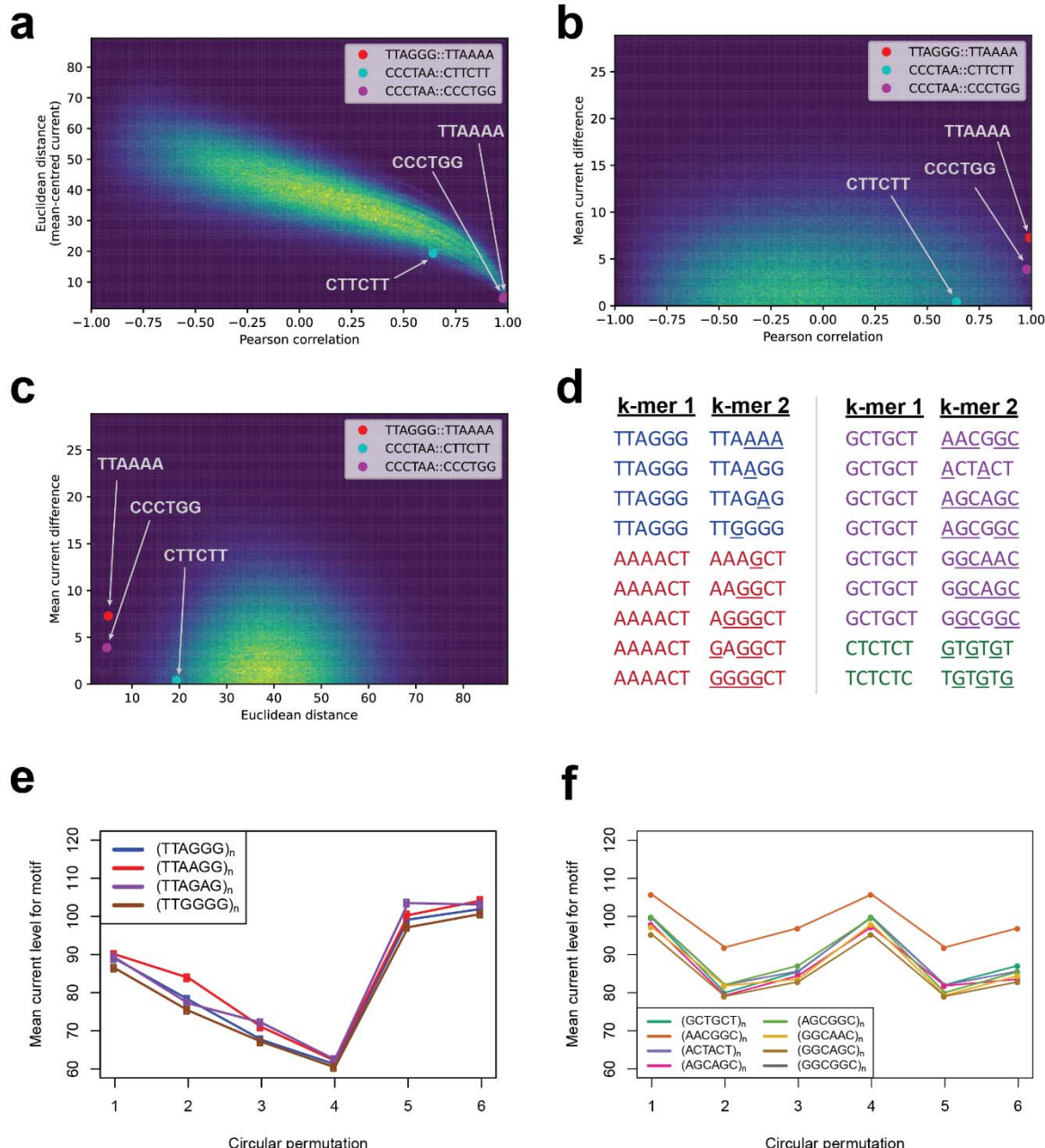
Supplementary Figure 7

Supplementary Figure 7 Similarities between current profiles for all possible pairs of 6-mer repeats. (a-c) Heatmaps depicting the Euclidean distances, Pearson correlation, and mean current differences between current profiles between all possible 6-mer repeat sequences. These are depicted as pairwise plots for **(a)** the Euclidean distances vs. the Pearson correlation, **(b)** the mean current difference vs. the Pearson correlation, and **(c)** the mean current difference vs. the Euclidean distance. The pairwise comparisons between the telomeric repeats and the observed basecalling repeat artifacts are also highlighted in the plots. **(d)** Example pairs of k-mer repeats with similar current profiles are as indicated. The nucleotides in k-mer 2 that differs from k-mer 1 is underlined to highlight the nucleotides that differ between the two types of

23

532 repeats. **(e-f)** Current profiles for repeats which were predicted to be highly similar to each other.
533 These are depicted for **(e)** TTAGGG telomeric repeats and telomere-like repeat sequences and
534 **(f)** GCTGCT repeat sequences that were highlighted in purple in Supplementary Figure 7d.
535
536

Supplementary Figure 8
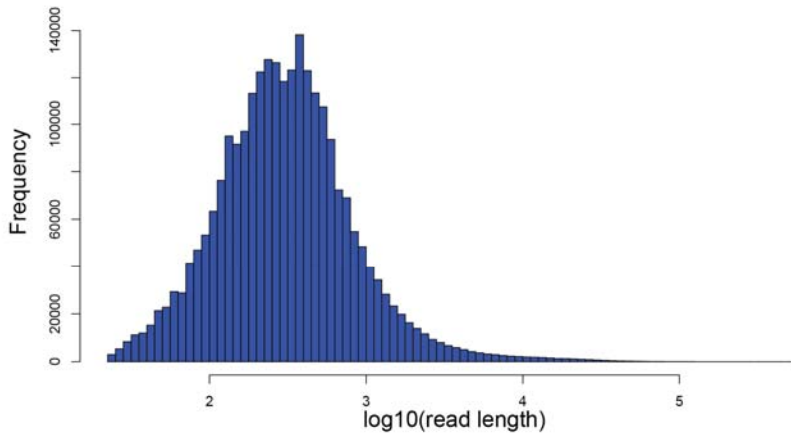
Supplementary Figure 8 Example of reads with $(GT)_n$ repeat sequences in the CHM13 dataset. (a-b) Two representative reads from the CHM13 nanopore sequencing dataset with $(GT)_n$ repeat sequences. **(c)** Read length distribution of unmappable $(GT)_n$ repeats (number of repeats $\geq$12) in the CHM13 nanopore dataset.

Supplementary Figure 9
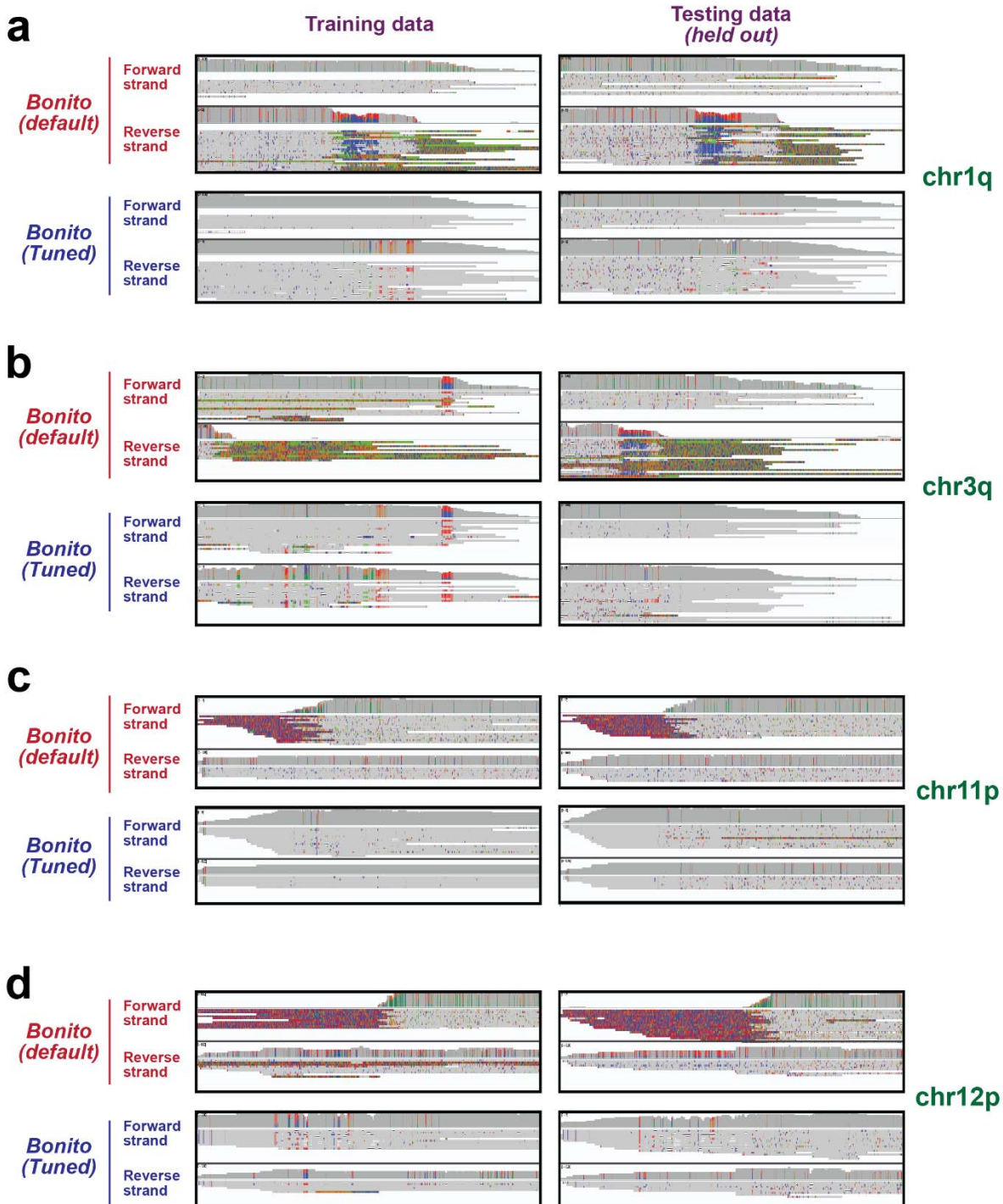
543
Supplementary Figure 9 Additional examples for the performance of the tuned bonito basecaller on telomeres on other chromosomal arms. The tuned model was applied to the training dataset used for model training, and on an additional held out test dataset that was not used during model training. IGV screenshots of the default and tuned bonito basecaller on the

548   training and testing dataset for the chromosomal arms **(a)** chr1q, **(b)** chr3q, **(c)** chr11p and **(d)**
549   chr12p are as depicted. Related to Figure 2b.
550
551

Supplementary Figure 10
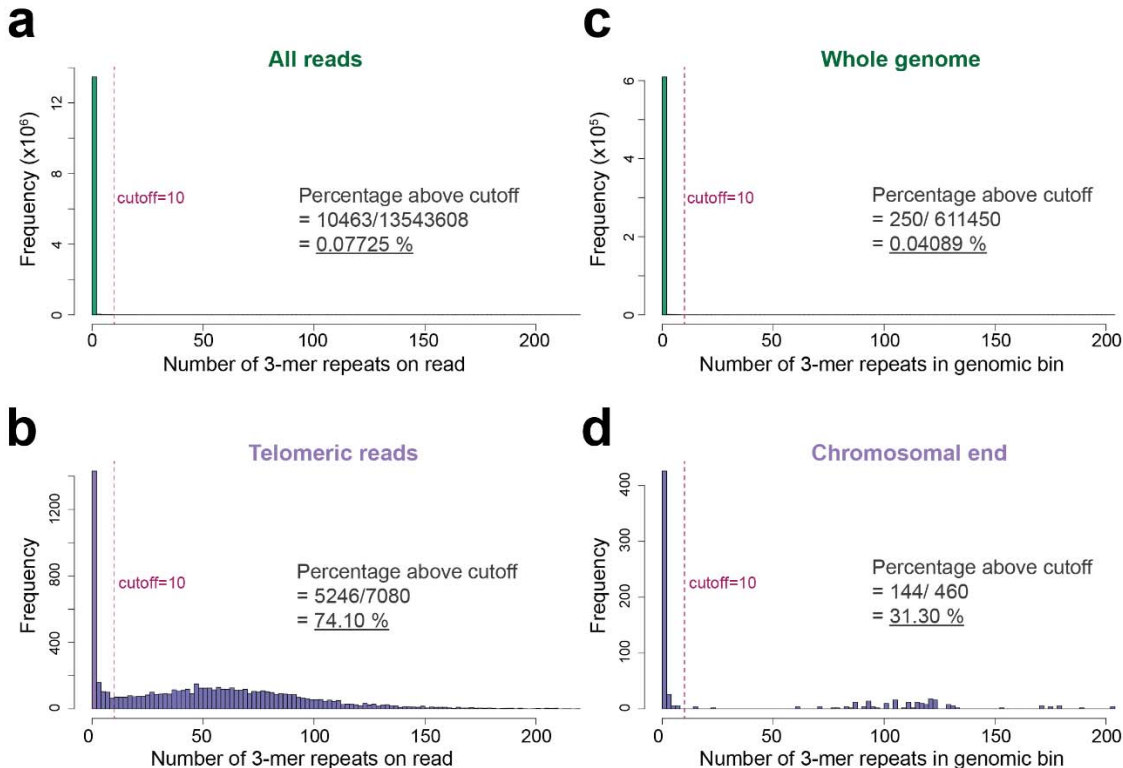
552
553 **Supplementary Figure 10 Histograms depicting the frequencies of 3-mer repeats on**
554 **reads at telomeres and on reads found at the rest of the genome in the CHM13 dataset.**
555 **(a-b)** The sum of 3-mer telomeric repeats $[(TTAGGG)_3 (CCCTAA)_3]$ and basecalling error
556 repeats $[(TTAAAA)_3, (TTTTAA)_3, (CTTCTT)_3, (AAGAAG)_3, (CCCTGG)_3, (CCAGGG)_3]$ on **(a-b)**
557 each long-read or **(c-d)** genomic bin are as depicted on the x-axis of each histogram. The
558 histograms represent the frequency of these repeats on **(a)** all long-reads in the CHM13 dataset,
559 **(b)** telomeric reads in the CHM13 dataset, **(c)** 20 kb genomic bins with 10 kb moving window for
560 the full CHM13 reference genome, **(d) a**nd for the 10 genomics bins on each chromosomal end
561 of the CHM13 genome.
562
563

564 **Supplementary Tables**

565

566 **Supplementary Table 1 List of k-mers with high similarities in current profiles.** The
567 pearson correlation, Euclidean distance, and mean current difference between each pair of k-
568 mer is as presented in the table.